Remote Sensing of Environment 138 (2013) 38–50

Contents lists available at SciVerse ScienceDirect

Remote Sensing of Environment

journal homepage: www.elsevier.com/locate/rse

A PRI-based water stress index combining structural and chlorophyll effects: Assessment using diurnal narrow-band airborne imagery and the CWSI thermal index

P.J. Zarco-Tejada [a,*], V. González-Dugo [a], L.E. Williams [b], L. Suárez [a], J.A.J. Berni [a], D. Goldhamer [c], E. Fereres [a,d]

[a] Instituto de Agricultura Sostenible (IAS), Consejo Superior de Investigaciones Científicas (CSIC), Alameda del Obispo s/n, 14004 Cordoba, Spain
[b] Department of Viticulture and Enology, UC-Davis and Kearney Agricultural Research and Extension Center, 9240 S. Riverbend Ave., Parlier, CA 93648, USA
[c] Department of Land, Air and Water Resources, University of California, Davis, CA 95616, USA
[d] Department of Agronomy, University of Cordoba, Campus Universitario de Rabanales, 14014 Cordoba, Spain

ARTICLE INFO

Article history:
Received 17 April 2013
Received in revised form 11 July 2013
Accepted 17 July 2013
Available online xxxx

Keywords:
PRI
CWSI
UAV
Narrow-band
Thermal
Airborne
Stress detection
Grapevines

ABSTRACT

This work advances the evaluation and interpretation of the Photochemical Reflectance Index (PRI) as an indicator of water stress, over a range of canopy structures and pigment content levels. Very high resolution (VHR) narrow-band multispectral (10 cm) and thermal (20 cm) imagery was acquired diurnally, in four airborne campaigns conducted over an experimental vineyard site undergoing three different irrigation treatments. Field measurements of leaf stomatal conductance (G_s) and leaf water potential (Ψ_{leaf}) were acquired concurrently with the airborne campaigns and compared against the Crop Water Stress Index (CWSI), a widely accepted, thermal-based indicator of water stress, and against narrow-band multispectral indices calculated from pure-vegetation pixels. The study proposes a new formulation, a normalized PRI (PRI_{norm}), in which the standard PRI index is normalized by an index that is sensitive to canopy structure (Renormalized Difference Vegetation Index, RDVI) and by a red edge index that is sensitive to chlorophyll content (R_{700}/R_{670}). The hypothesis investigated is that the new index, calculated as $PRI_{norm} = PRI/[RDVI \cdot R_{700}/R_{670}]$, not only detects xanthophyll pigment changes as a function of water stress, but also normalizes for the chlorophyll content level and canopy leaf area reduction induced by stress. Results demonstrated that when comparing PRI_{norm} against stomatal conductance ($r^2 = 0.79$; $p < 0.001$) and leaf water potential ($r^2 = 0.77$; $p < 0.001$) measured at midday, the new index performed better than the standard PRI ($r^2 = 0.52$ and 0.49, respectively). Further, when using the four flights conducted during the diurnal experiment, the relationships with stomatal conductance also showed the superior performance of PRI_{norm} ($r^2 = 0.68$) as opposed to PRI ($r^2 = 0.4$). The proposed normalized PRI was highly related ($r^2 = 0.75$; $p < 0.001$) to the thermal indicator of water stress, CWSI, which was used here as a benchmark. In comparison, the standard PRI index was found to be significantly related to CWSI ($p < 0.001$), although the relationship was weaker ($r^2 = 0.58$) than that obtained for PRI_{norm}. In summary, this study demonstrates that PRI_{norm} isolated better than PRI the physiological changes against a changing background of altered pigments and structure, tracking more precisely the diurnal dynamics of the stomatal aperture. Simulations conducted, using leaf and canopy radiative transfer models to elucidate these results, showed that PRI_{norm} is more linearly related to canopy pigment content than the standard PRI, and was more capable of differentiating between stress levels, providing better insight into the results of this diurnal study.

1. Introduction

The most established indicator of water stress derived from remote sensing imagery is the Crop Water Stress Index (CWSI) (Jackson, Idso, Reginato, & Pinter, 1981), which is calculated from thermal infrared data. The CWSI is based on the difference between canopy temperature and air temperature (T_c-T_a), normalized by the vapor pressure deficit (VPD). Jackson and co-workers (Idso, Jackson, Pinter, Reginato, & Hatfield, 1981; Idso, Jackson, & Reginato, 1978; Jackson et al., 1981) demonstrated that water stress induces stomatal closure, thereby decreasing evaporative cooling and increasing leaf temperature. The usefulness of the CWSI in vineyards located in the San Joaquin Valley of California was demonstrated by Grimes and Williams (1990). Midday measures of leaf water potential (Ψ_{leaf}) and yield were linearly related to the CWSI in that study as were several other means to determine vine water status.

Although the use of imagery was proposed back in the late 1970s, in operational terms it has not actually been used until more recently, mainly as a result of the widespread adoption of emerging technologies that integrate high-resolution thermal cameras on board small unmanned

* Corresponding author. Tel.: +34 957 499 280, +34 676 954 937; fax: +34 957 499 252.
E-mail address: pablo.zarco@csic.es (P.J. Zarco-Tejada).
URL: http://quantalab.ias.csic.es (P.J. Zarco-Tejada).

0034-4257/$ – see front matter © 2013 Elsevier Inc. All rights reserved.
http://dx.doi.org/10.1016/j.rse.2013.07.024

aerial vehicles (UAVs) (Berni, Zarco-Tejada, Suárez, & Fereres, 2009). In fact, several studies have shown that high resolution thermal imagery acquired from manned (Sepulcre-Cantó et al., 2006, 2007) or unmanned aerial platforms (Berni, Zarco-Tejada, Suárez et al., 2009; Berni, Zarco-Tejada, Sepulcre-Cantó, Fereres, & Villalobos, 2009; Gonzalez-Dugo et al., 2012; Zarco-Tejada, González-Dugo, & Berni, 2012) has enabled the detection of water stress by means of these miniaturized thermal cameras, delivering errors of less than 1 K in the estimation of surface temperature of pure vegetation, when the cameras have been duly radiometrically calibrated and atmospherically corrected (Berni, Zarco-Tejada, Suárez et al., 2009).

Whenever very high resolution (VHR) thermal imagery is not available, as in the case of existing thermal satellite imagery, Moran, Clarke, Inoue, and Vidal (1994) proposed a Water Deficit Index (WDI) based on the vegetation index/temperature (VIT) trapezoid approach, which is applicable to field crops with varying contributions of bare soil in the aggregated thermal pixel. This method was first proposed for use with alfalfa crops to enable the application of CWSI to mixed soil-vegetation pixels, and is mainly used for field crops and homogeneous canopies that gradually increase their leaf area and fractional cover over the growing season. Nevertheless, in the case of vineyards and other woody crop orchards, the large effects of bare soil and shadows cast by vegetation on the aggregated thermal pixel require the use of VHR imagery to extract pure vegetation pixels, and eliminate soil and other background effects (Leinonen & Jones, 2004). This is particularly critical when the objective is to apply deficit irrigation methods (for a review see Fereres & Soriano, 2007) with the required precision to enable real-time decisions. In such cases, thermal data extracted from pure vegetation pixels is required, as very small canopy temperature differences are found as a function of stress levels, i.e. in some cases approximately 1 K or less (see Zarco-Tejada et al., 2012, for an example of citrus orchards where differences of less than 1.2 K were found between deficit irrigation treatments).

Even though the usefulness of CWSI has been demonstrated in a number of studies on monitoring water deficit levels, alternative narrow-band indices calculated in the visible and in the red edge spectral region have also been proposed to detect water stress (Zarco-Tejada et al., 2012). These new methods focus mainly on: i) the epoxidation state of xanthophyll cycle pigments, using the Photochemical Reflectance Index (PRI) (Gamon, Peñuelas, & Field, 1992), which serves as a proxy for water stress detection (Peguero-Pina, Morales, Flexas, Gil-Pelegrín, & Moya, 2008; Suarez, Zarco-Tejada, Berni, González-Dugo, & Fereres, 2009; Suarez et al., 2008; Suarez et al., 2010; Thenot, Méthy, & Winkel, 2002); and ii) solar-induced chlorophyll fluorescence emission (Flexas, Briantais, Cerovic, Medrano, & Moya, 2000; Flexas, Escalona, & Medrano, 1999; Flexas et al., 2002; Moya et al., 2004), which has been shown to be linked with stomatal conductance under water stress conditions. In fact, since the 1970s, there have been several studies that have demonstrated the link between fluorescence and photosynthesis, as well as other plant physiological processes (Krause & Weis, 1984; Larcher, 1994; Lichtenthaler, 1992; Lichtenthaler & Rinderle, 1988; Papageorgiou, 1975; Schreiber & Bilger, 1987; Schreiber, Bilger, & Neubauer, 1994).

The justification for focusing on indicators other than the thermal infrared indices is twofold: first, although canopy temperature may be a direct indicator of canopy transpiration, it does not account directly for other physiological changes such as photosynthetic pigment changes (occurring to chlorophyll, carotenoids, and xanthophylls), or non-stomatal reductions of photosynthesis under water stress conditions. Furthermore, the diurnal patterns of stomatal conductance in some plants are such that the relationships between canopy temperature and stress are not clear-cut. In some species, high vapor pressure deficits induce a continuous decline in leaf conductance, starting in the early morning hours, even when trees are well supplied with water (Fereres, Cruz-Romero, Hoffman, & Rawlins, 1979; Hall, Camacho-B, & Kaufmann, 1975; Villalobos, Testi, & Moreno-Perez, 2008). Although stomatal conductance and photosynthesis are linked, they may change at different rates under deficit irrigation conditions and during recovery following periods of water stress (Jones, 1992; Miyashita, Tanakamaru, Maitani, & Kimura, 2005). For these reasons, temperature-derived indicators would underestimate the net effect of severe water stress on assimilation and growth and thus, a water stress index that is sensitive to photosynthetic rates, as well as to transpiration, may be advantageous.

A further reason for endeavoring to find indicators other than the CWSI to detect water stress is related solely to practical and operational aspects: unfortunately, current and near-future satellite missions will not provide VHR thermal imagery for global monitoring of vegetation. Furthermore, the current and future satellite thermal sensors planned for civil remote sensing applications are still very far from providing the required high resolution needed to monitor heterogeneous canopies on a global scale. By way of example, the latest Landsat Data Continuity Mission (LDCM), launched only recently in February 2013, delivers two thermal infrared bands at 100 m resolution, and although it is useful for certain global monitoring studies, the low resolution of the thermal bands is a clear limitation when the aim is to monitor heterogeneous canopies, or apply precision agriculture methods. Technical and security reasons prevent the launch of higher resolution thermal satellite sensors, i.e. with resolutions of approximately 1 m or less. In this sense, alternatives based on multispectral imagery would be technically compatible with the current capabilities of narrow-band multispectral satellite sensors, which will eventually provide VHR maps of physiological indices related to photosynthetic pigments such as carotenoids and chlorophyll content (Haboudane, Miller, Tremblay, Zarco-Tejada, & Dextraze, 2002; Zarco-Tejada, Guillén-Climent et al., 2013), or even chlorophyll fluorescence (Damm et al., 2011; Meroni, Colombo, & Cogliati, 2004; Meroni, Picchi et al., 2008; Meroni, Rossini, Guanter et al., 2009; Meroni, Rossini et al., 2008; Moya et al., 2004; Zarco-Tejada et al., 2012).

The sensitivity of PRI for water stress detection has been proven in recent studies (Peguero-Pina et al., 2008; Suarez et al., 2008, 2009, 2010; Thenot et al., 2002; Zarco-Tejada et al., 2012) However, it has also been documented that there are certain issues with this index, i.e. the viewing and illumination geometry effects, crown architecture, and shadow/sunlit fraction (Barton & North, 2001; Hall et al., 2008; Hilker et al., 2008; Middleton et al., 2009; Suarez et al., 2008); accordingly, new formulations for PRI using alternative reference bands were proposed recently in an attempt to minimize these structural effects (Hernández-Clemente, Navarro-Cerrillo, Suárez, Morales, & Zarco-Tejada, 2011; Stagakis, González-Dugo, Cid, Guillén-Climent, & Zarco-Tejada, 2012). Other confounding factors of PRI that have not yet been assessed are chlorophyll and carotenoid absorption, which overlap with the spectral bands sensitive to xanthophyll pigments. Although most of the recent studies on PRI have been conducted on canopies that have very little variation in their structural and pigment concentration, and were grown using regulated deficit irrigation techniques (Stagakis et al., 2012; Suarez et al., 2008, 2009, 2010), further progress is required to elucidate the temporal and spatial dynamics of PRI on pixels in the presence of varying concentrations of xanthophyll, chlorophyll, anthocyanins, and carotenoid pigments, or different structural levels.

Along the lines that progress on narrow-band remote sensing chlorophyll indices has evolved to ensure less sensitivity to structural effects, as in the case of the family of indices based on the Chlorophyll Absorption in Reflectance Index (CARI) and its transformations into TCARI & MCARI normalized by OSAVI in the form TCARI/OSAVI (Haboudane et al., 2002), this paper proposes a PRI-based index, normalized by canopy chlorophyll content, using a combination of a structural index (RDVI) that is less sensitive to leaf area index saturation (Rougean & Breon, 1995), and the R_{700}/R_{670} index that is sensitive to chlorophyll content, which is potentially affected by chlorophyll fluorescence emission. The hypothesis under study is that a PRI index normalized by canopy chlorophyll content would improve its sensitivity to variations in canopy stomatal conductance, thereby becoming a more robust indicator of the diurnal dynamics of water stress. The work was

based on VHR narrow-band multispectral and thermal imagery acquired in four diurnal airborne campaigns over a vineyard study site undergoing three different irrigation treatments. The assessment evaluated the relationships between the proposed new PRI formulation, and field-measured stomatal conductance and water potential. Relationships with CWSI, which was used as a remote sensing benchmark for water stress detection, are also discussed herein.

2. Materials and methods

2.1. Study site description

The experiment took place in summer 2009 in a 1.4 ha experimental vineyard (*Vitis vinifera* L. cv. Thompson Seedless) located at the University of California Kearney Agricultural Research and Extension Center, Parlier, California (USA) (36°48′N, 119°30′W). The vine trellis was comprised of 2.13 m wooden stakes driven into the soil to a depth of 0.45 m at each vine; a 0.6-m cross-arm was placed atop each stake and wires were attached to either end of the cross-arms. Further details of the study site can be found in Williams, Baeza, and Vaughn (2012). The soil on the site is a Handford fine sandy loam, classified as Typic Torriorthents. Vines were manually irrigated 5 days a week via drip irrigation. Irrigation requirements were calculated according to established crop coefficients previously obtained from an on-site weighing lysimeter (Williams, Phene, Grimes, & Trout, 2003). Reference ET (ET_o) was obtained from a California Irrigation Management Information System (CIMIS) weather station #39 located 2 km from the vineyard site. Three blocks within the vineyard (non-irrigated (NI), Fig. 1) were rainfed throughout the entire season. A second, intermediate (INT) treatment was designed in which irrigation was terminated two weeks prior to the start of the airborne campaigns. Three further blocks were chosen randomly from the remainder of the well-irrigated vineyard for the purpose of conducting measurements (IRR treatment; Fig. 1).

Field measurements of leaf stomatal conductance (G_s) and leaf water potential (Ψ_{leaf}) were made concurrently with acquisition of airborne imagery over the experimental field. Leaf Ψ was measured in the central row of each block at the time of flights according to the procedure outlined by Williams and Araujo (2002). Three leaves were selected for measurement from along the row using a pressure chamber (model 1000; PMS instruments, Corvallis, OR, USA). Pre-dawn leaf water potential (Ψ_{PD}) was measured prior to sunrise. Around the time of each flight, stomatal conductance was measured using a leaf porometer (SC-1, Decagon Devices, Pullman, WA, USA) on six fully developed leaves per block that were exposed to direct solar radiation in the central row. Soil water content was measured as described by Williams and Trout (2005) in order to estimate grapevine water use of the irrigated (IRR) and non-irrigated (NI) treatments using soil water budgeting as described by Williams, Grimes, and Phene (2010).

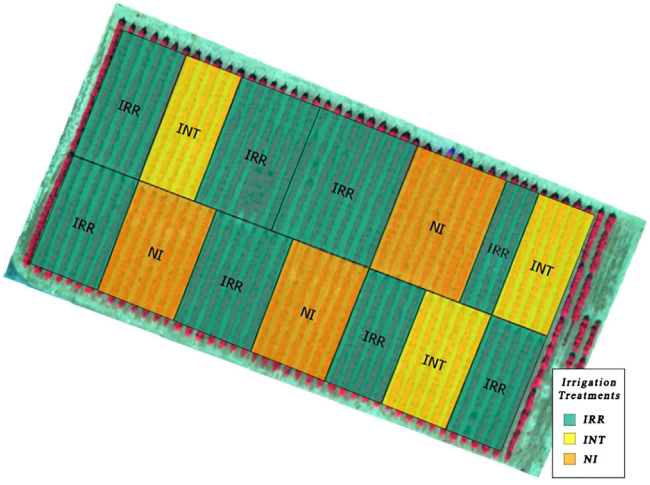

Fig. 1. Overview of the experimental vineyard used in this study. Plots with the three irrigation treatments are represented by colors, as indicated. IRR refers to well irrigated; NI is the non-irrigated treatment (rainfed); an intermediate treatment (INT) was designed, in which irrigation stopped two weeks prior to the airborne campaigns. (For interpretation of the references to color in this figure legend, the reader is referred to the web version of this article.)

2.2. Airborne campaigns

A total of four flights were conducted at 10:00, 13:00, 15:30, and 18:00 h, local time (PST) on 2 July 2009 concurrently with field data collection, using both a multispectral and a thermal camera on board an Unmanned Aerial Vehicle (UAV). The instruments were operated by the Laboratory for Research Methods in Quantitative Remote Sensing (Quantalab, IAS-CSIC, Spain) (Berni, Zarco-Tejada, Suárez et al., 2009; Zarco-Tejada, González-Dugo et al., 2012; Zarco-Tejada, Guillén-Climent et al., 2013), as part of a collaborative research project between the Spanish Council for Scientific Research (CSIC) and the University of California, Davis (UCD), USA. The UAV used in the airborne campaigns was a 2 m wingspan, fixed-wing platform, with a 5.8 kg take-off weight (TOW) (mX-SIGHT, UAV Services and Systems, Germany) and flight endurance of 1 h. The flights were conducted at an average height of 150 m above ground level and 70 km/h speed. The UAV was controlled by an autopilot system (AP04, UAV Navigation, Madrid, Spain) that enabled autonomous navigation, based on coordinates programmed during mission planning. The autopilot system was equipped with a dual CPU, controlling an integrated Altitude Heading Reference System (AHRS) based on an L1 GPS board, 3-axis accelerometers, yaw rate gyros, and a 3-axis magnetometer (Berni, Zarco-Tejada, Suárez et al., 2009). The remote sensing multispectral and thermal cameras on

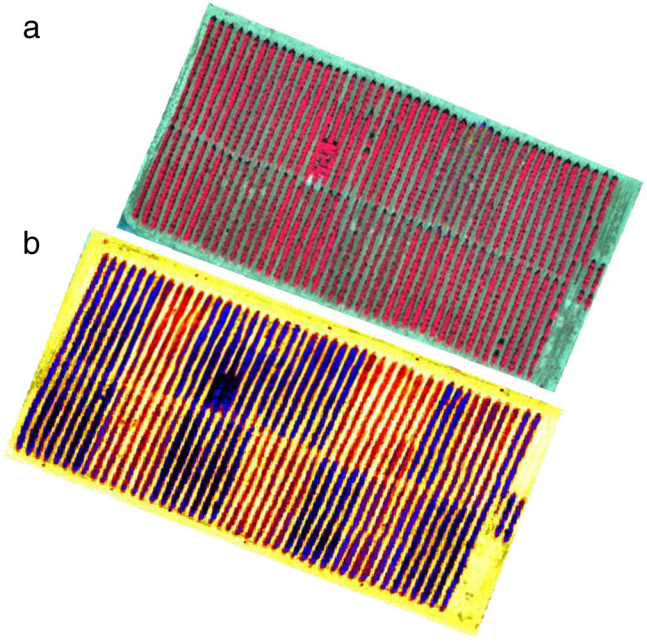

Fig. 2. Multispectral image acquired at 13.00 h from the unmanned aerial vehicle (UAV) yielding 10 cm resolution and 6 spectral bands at 10 nm FWHM observing the vineyard site used for field data collection (a); the same experimental field was imaged using a high resolution thermal camera, acquiring the imagery at 20 cm pixel size (b). The high resolution used enabled the extraction of pure-vine reflectance and temperature from each irrigation block at each of the four flight times. The continuous bright red rectangular area in (a) or bright blue/purple area in (b) is the location of the weighing lysimeter in this vineyard. Vines in the lysimeter and immediate surrounding area were trained to an overhead arbor trellis, therefore a continuous canopy between rows at that location. Vines in the lysimeter were being irrigated at 100% of measured ET_c as described by Williams et al. (2003). (For interpretation of the references to color in this figure legend, the reader is referred to the web version of this article.)

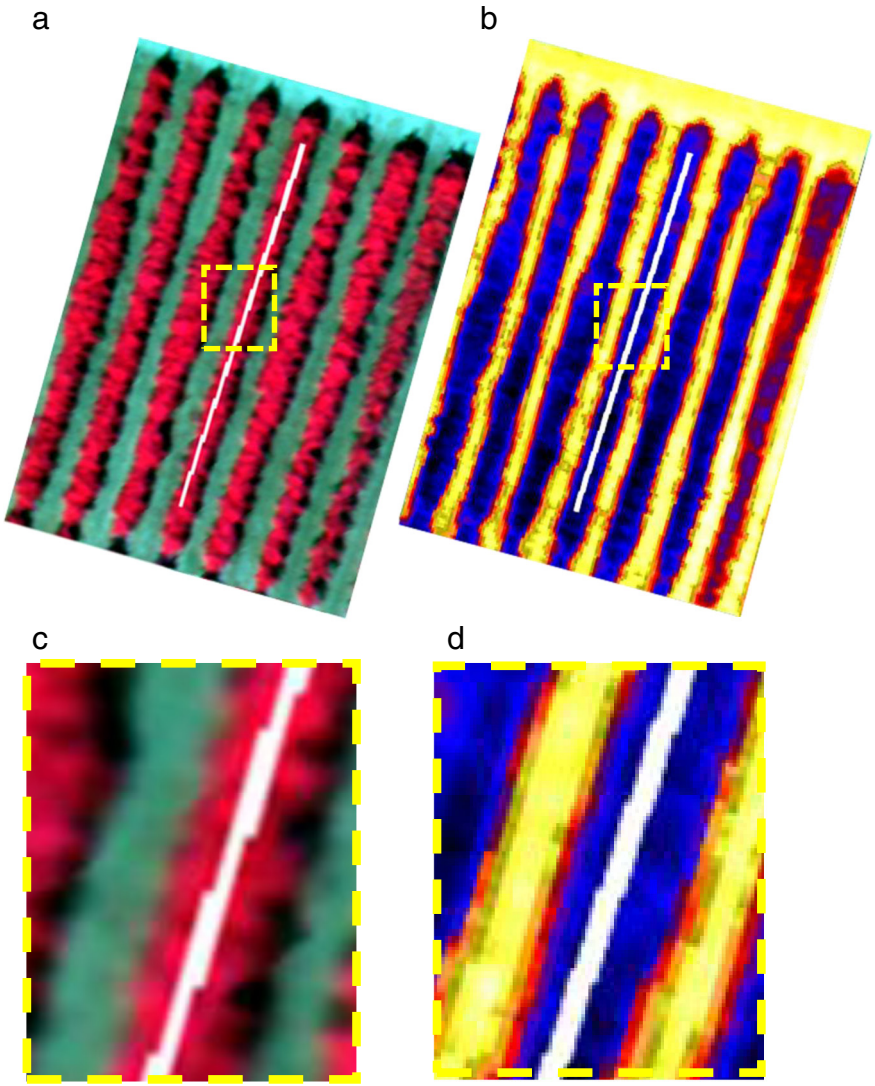

Fig. 3. Identification of pure-vine pixels extracted from the center of the rows (white line) and used to calculate all reflectance indices (a;c), and T_c-T_a and CWSI from the thermal image (b;d). Acquired high resolution imagery enabled extraction of the water-stress indices with no shadow or background effects.

board the UAV were operated by means of a radio link to a ground station.

The SixCam multispectral camera (QuantaLab-IAS-CSIC, Córdoba, Spain) comprised six independent image sensors with user-configurable spectral filters (Berni, Zarco-Tejada, Suárez et al., 2009), and 2592 × 1944 pixels with 10-bit radiometric resolution. With an optics focal length of 8.4 mm and angular field of view (FOV) of 38.04° × 28.53°, the camera yielded 10 cm spatial resolution. The multispectral images acquired over the vineyard field enabled identification of pure vines; accordingly, each experimental block could be distinguished (Fig. 2a). The spectral bandset selected for this study comprised center wavelengths at 530, 550, 570, 670, 700 and 800 nm acquired at 10 nm full-width at half-maximum (FWHM), which were subsequently used for computing the vegetation indices described herein.

The camera was radiometrically calibrated in the laboratory using a uniform calibration body (integrating sphere, CSTM-USS-2000C Uniform Source System, LabSphere, NH, USA) set for four different levels of illumination and eleven integration times. Radiance values were converted to reflectance using the total incoming irradiance simulated with SMARTS (Gueymard, 2005) using Microtops II sunphotometer data (Solar Light Co., Philadelphia, PA, USA) collected in the study area at the time of each flight to derive aerosol optical depth (AOD)

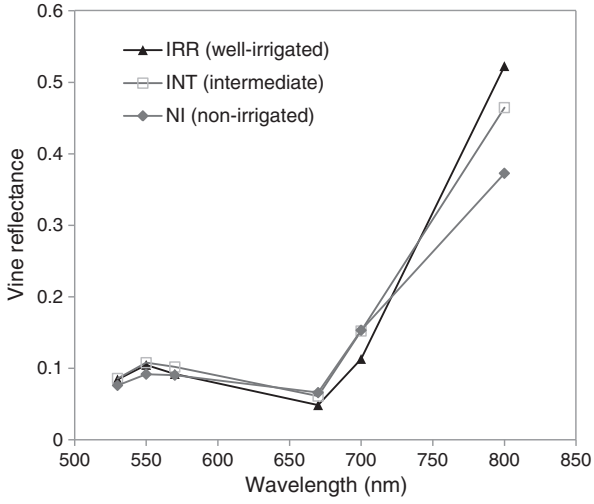

Fig. 4. Mean reflectance extracted from the airborne multispectral imagery acquired at 13:00 h over the experimental site, showing the mean spectra calculated from pure-vine pixels for the IRR (well-irrigated), non-irrigated (NI), and intermediate (INT) treatments.

Table 1
Narrow-band multispectral indices used in this study.

Index	Equation	Reference
Structural indices		
NDVI	$NDVI = (R_{800} - R_{670})/(R_{800} + R_{670})$	Rouse et al. (1974)
RDVI	$RDVI = (R_{800} - R_{670})/(R_{800} + R_{670})^{0.5}$	Rougean and Breon (1995)
Chlorophyll indices		
TCARI	$TCARI = 3 \cdot [(R_{700} - R_{670}) - 0.2 \cdot (R_{700} - R_{550}) \cdot (R_{700}/R_{670})]$	Haboudane et al. (2002)
TCARI/OSAVI	$TCARI/OSAVI = [3 \cdot [(R_{700} - R_{670}) - 0.2 \cdot (R_{700} - R_{550}) \cdot (R_{700}/R_{670})]]/[(1 + 0.16) \cdot (R_{800} - R_{670})/(R_{800} + R_{670} + 0.16)]$	Haboudane et al. (2002)
Red edge ratio index	R_{700}/R_{670}	Part of TCARI index
Xanthophyll indices		
PRI_{570}	$PRI_{570} = (R_{570} - R_{531})/(R_{570} + R_{531})$	Gamon et al. (1992)
PRI_{norm}	$PRI_{norm} = PRI_{570}/[RDVI \cdot (R_{700}/R_{670})]$	This study

Table 2
Leaf water potential (Ψ_{leaf}, MPa) and stomatal conductance (G_s, mmol m^{-2} s^{-1}) measured at each flight time (h, Pacific Daylight Time) except when Ψ_{leaf} was measured prior to sunrise (pre-dawn, measured at 05:00 h). For each variable and time, values followed by a different letter are significantly different ($p < 0.05$; $n = 3$).

	Treatment	Pre-dawn	10:00	13:00	15:30	18:00
Ψ_{leaf}	IRR	−0.04 a	−0.46 a	−0.72 a	−0.71 a	−0.60 a
	INT	−0.27 b	−0.82 b	−1.11 b	−1.05 b	−0.87 b
	NI	−0.48 c	−0.95 c	−1.20 c	−1.19 c	−0.99 b
G_s	IRR	–	241 a	291 a	271 a	164 a
	INT	–	154 b	110 b	71 b	43 b
	NI	–	89 b	44 c	31 c	32 b

at 550 nm; this model has been used previously in other studies, e.g. Berni, Zarco-Tejada, Suárez et al. (2009), Suarez et al. (2010) and Guillén-Climent, Zarco-Tejada, Berni, North, and Villalobos (2012). Both the data obtained from the airborne campaign and sunphotometer data were collected under clear sky conditions. The sunphotometer was connected to a GPS-12 model (Garmin, Olathe, KS, USA) to obtain simultaneous readings of the solar geometry at the time of the spectral acquisitions.

The thermal camera used in this experiment (MIRICLE 307, Thermoteknix Systems Ltd, Cambridge, UK) was equipped with a 14.25 mm f1.3 lens, yielding a 20 cm resolution imagery. The image sensor was a Focal Plane Array (FPA), based on uncooled microbolometers, with a spectral range of 8–12 μm, yielding a 25 μm pixel size. The camera acquired 640 × 480 thermal images at 14-bit resolution; radiometric calibration was conducted in the laboratory using blackbodies at varying target and ambient temperatures in order to develop radiometric calibration algorithms, as well as internal calibration for non-uniformity correction (NUC). The thermal images enabled identification of each treatment block under study (Fig. 2b). Local atmospheric conditions at the time of each flight were established by measuring air temperature, relative humidity, and barometric pressure, using a portable weather station (Model WXT510, Vaisala, Finland) located in the middle of the experimental vineyard.

The high resolution multispectral and thermal imagery acquired by the UAV platform enabled identification of each individual treatment block (Fig. 2a;b), and also, the extraction of pure vine reflectance and pure vine temperature, with small mixing effects due to soil and shadows (Fig. 3). For each treatment block, a region of interest (ROI) was established in the center of each vine row to extract pure vine reflectance (Fig. 3a;c), and pure vine temperature (Fig. 3b;d), using only pure vegetation pixels. The image reflectance spectra extracted from each treatment block, coinciding with each flight time, were subsequently used to compute the vegetation indices used in the analysis. Fig. 4 shows the mean pure-vine reflectance for each of the three treatments (IRR, INT, NI) extracted from the midday flight (13:00 h), showing a consistent variation of reflectance at the near infrared (NIR), red edge, and visible region, as a function of the growth and imposed stress levels.

Table 3
Relationships between structural (NDVI, RDVI), chlorophyll (TCARI, TCARI/OSAVI, R_{700}/R_{670}), photochemical reflectance indices (PRI, PRI_{norm}) and thermal indicators (T_c-T_a, CWSI), and stomatal conductance (G_s) and leaf water potential (Ψ_{leaf}) for a) 13:00 h; b) 13:00 + 15:30 h; and c) four flights.

	G_s (mmol · m^{-2} · s^{-1})			Ψ_{leaf} (MPa)		
	13:00 h (n = 9)	13:00 h + 15:30 h (n = 18)	10:00 h + 13:00 h + 15:30 h + 18:00 h (n = 36)	13:00 h (n = 9)	13:00 h + 15:30 h (n = 18)	10:00 h + 13:00 h + 15:30 h + 18:00 h (n = 36)
Structural						
NDVI	0.63*	0.33*	0.21**	0.34	0.38**	0.03
RDVI	0.7**	0.28*	0.11*	0.49*	0.38**	0.01
Chlorophyll						
TCARI	0.14	0.2	0.12	0.13	0.1	0.11
TCARI/OSAVI	0.01	0.02	0.01	0.01	0.01	0.05
R_{700}/R_{670}	0.16	0.23*	0.21**	0.14	0.15	0.17
Photochemical						
PRI	0.49*	0.52***	0.4***	0.53*	0.49**	0.37***
PRI_{norm}	0.81***	0.79***	0.68***	0.82***	0.77***	0.44***
Thermal						
T_c-T_a	0.74**	0.75***	0.59***	0.95***	0.76***	0.57***
CWSI	0.74**	0.77***	–	0.95***	0.78***	–

* $p < 0.05$.
** $p < 0.01$.
*** $p < 0.001$.

2.3. Physiological and structural indices calculated from the airborne imagery

Indices related to leaf physiological condition and canopy structure were calculated from the imagery (Table 1). The structural indices were calculated to assess whether the effects of water-stress on the vine structure could be captured by the Normalized Difference Vegetation Index, $NDVI = (R_{800} - R_{670})/(R_{800} + R_{670})$ (Rouse, Haas, Schell, Deering, & Harlan, 1974), with a modification of NDVI to increase its sensitivity, in the form of the Renormalized Difference Vegetation Index, $RDVI = (R_{800} - R_{670})/\sqrt{(R_{800} + R_{670})}$ (Rougean & Breon, 1995), and using other widely used ratios, e.g. the Optimized Soil-Adjusted Vegetation Index, $OSAVI = ((1 + 0.16)\cdot(R_{800} - R_{670})/(R_{800} + R_{670} + 0.16))$ (Rondeaux, Steven, & Baret, 1996). In this case, the selected chlorophyll a + b indices were: the Transformed Chlorophyll Absorption in Reflectance Index (TCARI) (Haboudane et al., 2002); the aforementioned TCARI, normalized by OSAVI to obtain TCARI/OSAVI, as proposed by Haboudane et al. (2002) and used by Meggio et al. (2010); and the red edge ratio index R_{700}/R_{670}, which is sensitive to the chlorophyll absorption that forms part of the TCARI index. The Photochemical Reflectance Index (PRI) was calculated using the 570 nm band as a reference (Gamon et al., 1992) in the form $PRI = (R_{570} - R_{531})/(R_{570} + R_{531})$.

As part of this study, the PRI index was normalized by canopy chlorophyll content, which was calculated as the combination of the RDVI structural index and the red edge index R_{700}/R_{670}, the new index being referred to herein as PRI_{norm}. The hypothesis is that the new index, calculated as $PRI_{norm} = PRI/[RDVI \cdot R_{700}/R_{670}]$, would account for xanthophyll pigment changes as a function of water stress, and at the same time, would also be sensitive to the effects of canopy chlorophyll content and leaf area levels on the R_{700}/R_{670} and RDVI indices.

2.4. Calculation of CWSI from thermal imagery

The mean pure-vine temperature (T_c), extracted from the images, and air temperature (T_a) were used to calculate the Crop Water Stress Index (CWSI), according to the methodology proposed by Idso et al. (1981).

$$CWSI = \frac{(Tc\text{-}Ta) - (Tc\text{-}Ta)_{LL}}{(Tc\text{-}Ta)_{UL} - (Tc\text{-}Ta)_{LL}} \quad (1)$$

where $(T_c\text{-}T_a)_{LL}$ is the lower limit of the differential between canopy and air temperature, and corresponds to the value of a canopy transpiring at the potential rate, where $(T_c\text{-}T_a)_{UL}$ corresponds to the upper limit, i.e. the value of a canopy where transpiration is completely halted. The Non-Water-Stress-Baseline (NWSB) is defined by the relationship between the $T_c\text{-}T_a$ of a well-irrigated vine and the vapor pressure deficit (VPD), with the LL being set for a given evaporative demand. The NWSB used in this study was determined by Grimes and Williams (1990) in this vineyard ($T_c\text{-}T_a = 0.695 - 1.575 \cdot VPD$). The UL is calculated as the intercept of the NWSB in an oversaturated atmosphere for a given negative VPD, in order to overcome the fact that the $T_c\text{-}T_a$ value is positive and different from 0 (Idso et al., 1981). The calculation of CWSI was restricted to flights conducted at 13:00 and 15:30, coinciding with the times at which the NWSB was originally obtained.

3. Results

The statistical analysis conducted between the multispectral and thermal indices calculated from the airborne imagery (Table 1), and the G_s and Ψ_{leaf} measured in the field for each irrigation treatment (Table 2) at the different flight times, is shown in Table 3. The field

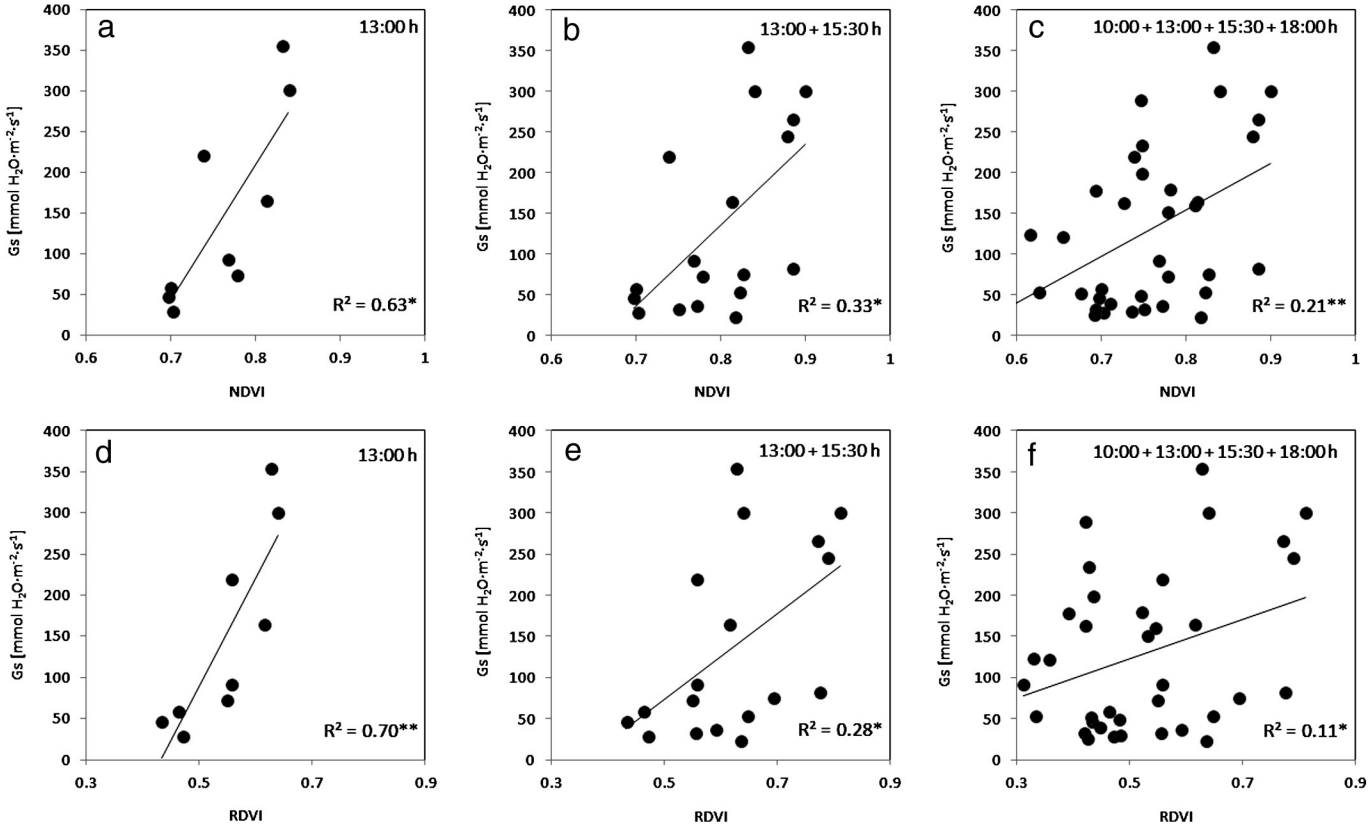

Fig. 5. Relationships obtained between stomatal conductance (G_s) and NDVI (a;b;c) and RDVI (d;e;f) for the flight conducted at 13:00 h (a;d), for the two midday flights (b;e) and for all four flights aggregated (c;f). Statistical significance is indicated as * ($p < 0.05$), ** ($p < 0.01$), and *** ($p < 0.001$).

measurements conducted at each flight time showed significant differences among the three irrigation treatments in most cases. In particular, there were significant differences in Ψ_{leaf} among irrigation treatments at all times it was measured, except for the last sample time (18:00 h). There were also significant differences in G_s among the three irrigation treatments, with the lowest values occurring in the NI treatment. Signs of recovery in Ψ_{leaf} were detected in all three treatments at the 18:00 h sample time; however, G_s values did not recover by that time (Table 2). Grapevine water use for the period from 26 June through 2 July was equivalent to 5.84 and 1.54 mm d^{-1} for the IRR and NI treatments, respectively.

Table 3 compares the relationships obtained for all indices: solely for the midday flight (13:00 h); for the two mid-day flights (13:00 h + 15:30 h); and for the four flights together, including the morning (10:00 h) and afternoon (18:00 h) flights. A separate analysis was made for the central hours, and likewise, for all flights together, in order to determine the effects of the viewing geometry on the relationships over the diurnal course, and also, to assess the sensitivity of the indices on single flights only, as compared to the entire diurnal dataset.

Due to the large structural effects (smaller canopies) caused by the long-term water stress imposed in the NI treatment, compared to the well-watered treatments, the relationship between G_s and the structural indices (NDVI, RDVI) was strong for the midday flight (13:00 h) ($r^2 = 0.63$, $p < 0.05$ for NDVI, Fig. 5a; $r^2 = 0.7$, $p < 0.01$ for RDVI, Fig. 5d). The correlation diminished when data from other flight times were included, obtaining weaker results for the two midday flights together (13:00 + 15:30 h) ($r^2 = 0.33$ for NDVI, Fig. 5b; $r^2 = 0.28$ for RDVI, Fig. 5e; $p < 0.05$ in both cases). When all flights were analyzed

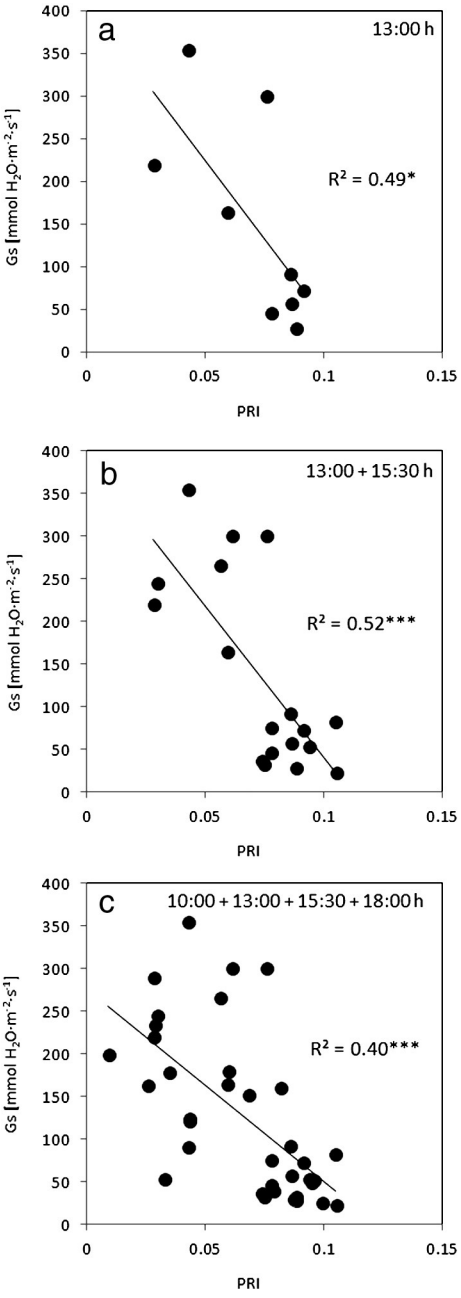

Fig. 6. Relationships obtained between stomatal conductance (G_s) and PRI for the flight conducted at 13:00 h (a), for the two midday flights (b) and for all four flights aggregated (c). Statistical significance is indicated as * ($p < 0.05$), ** ($p < 0.01$), and *** ($p < 0.001$).

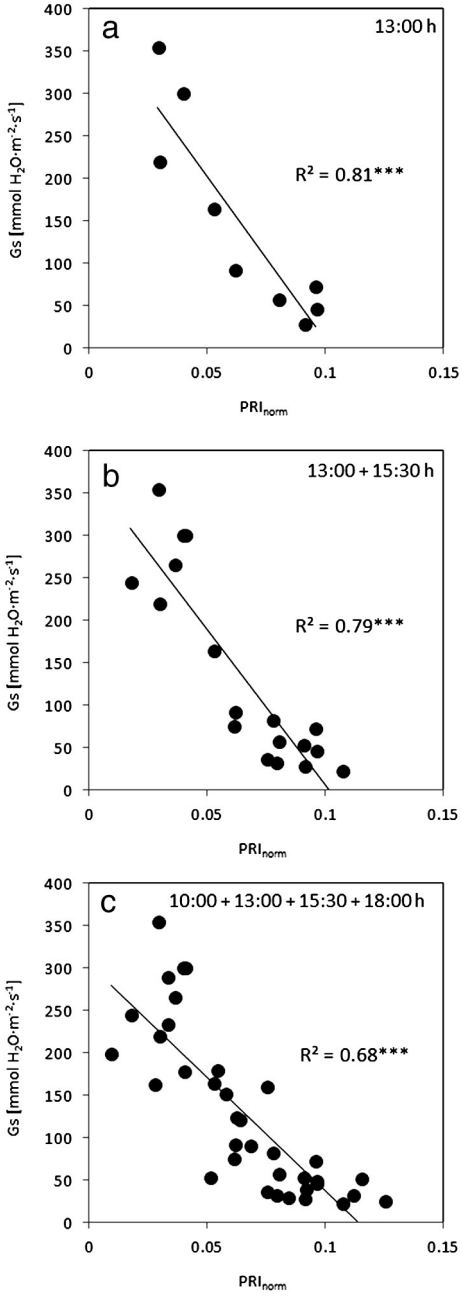

Fig. 7. Relationships obtained between stomatal conductance (G_s) and the normalized PRI index proposed in this study (PRI_{norm}) for the flight conducted at 13:00 h (a), for the two midday flights (b) and for all four flights aggregated (c). Statistical significance is indicated as * ($p < 0.05$), ** ($p < 0.01$), and *** ($p < 0.001$).

together (10:00 + 13:00 + 15:30 + 18:00 h), results showed a significant, albeit weak, coefficient of determination for the structural indices vs the diurnal variation of stomatal conductance ($r^2 = 0.21$ for NDVI, Fig. 5c; $r^2 = 0.11$ for RDVI, Fig. 5f). The sensitivity of NDVI and RDVI proved to be consistent at both 13:00 h and 15:30 h flight times, showing RDVI to be slightly better related to stomatal conductance than NDVI (in both cases, $r^2 = 0.63$ for NDVI ($p < 0.05$), and $r^2 = 0.7$ for RDVI ($p < 0.01$)).

As a result of the large structural effects observed between treatments during the experiment, the relationships obtained at 13:00 h between PRI and G_s were weaker than for the structural indices NDVI and RDVI (Fig. 6). Nevertheless, PRI captured the diurnal variation of G_s better than NDVI and RDVI, when analyzing all flights together. The sensitivity of PRI was comparable for the midday flight (13:00 h) ($r^2 = 0.49$, $p < 0.05$, Fig. 6a), and for both midday flights together ($r^2 = 0.52$; $p < 0.001$, Fig. 6b). Therefore, sensitivity decreased less for PRI than for the structural indices, NDVI and RDVI, when the two midday flights were taken together. The relationship between PRI and G_s diminished slightly when the data from all four flights were analyzed together, showing a weaker, albeit significant, relationship ($r^2 = 0.4$, $p < 0.001$, Fig. 6c). In comparison, RDVI yielded a weak $r^2 = 0.11$ ($p < 0.05$), showing that it was highly affected by the diurnal course of the experiment.

The proposed PRI-based index normalized by structure (RDVI) and by the red-edge chlorophyll ratio (R_{700}/R_{670}), performed better than the structural indices alone (NDVI; RDVI), and than the standard PRI formulation for the midday flight (13:00 h) ($r^2 = 0.81$, $p < 0.001$, Fig. 7a); the two midday flights together (13:00 + 15:30 h) ($r^2 = 0.79$, $p < 0.001$, Fig. 7b); and even when data from all four flights were analyzed together ($r^2 = 0.68$, $p < 0.001$, Fig. 7c). The relationships with G_s were better for the new PRI-based index when normalized by both structural (RDVI) and chlorophyll (R_{700}/R_{670}) indices, than when PRI was used in combination with only the structural (RDVI) index (data not shown). Moreover, PRI normalized by RDVI and R_{700}/R_{670} obtained $r^2 = 0.81$ at 13:00 h, and $r^2 = 0.79$ for the two midday flights, whereas PRI normalized only by the RDVI was significantly related but less sensitive, yielding $r^2 = 0.7$ at 13:00 h, and $r^2 = 0.64$ for the two midday flights together. This was due to the fact that, as shown in Table 3, R_{700}/R_{670} evidenced some sensitivity to stomatal conductance, yielding coefficients of determination ranging from $r^2 = 0.23$, $p < 0.05$ (13:00) to $r^2 = 0.21$, $p < 0.01$ (all flights together), and performing better than TCARI. Although this sensitivity of R_{700}/R_{670} to G_s might be considered marginal, the resulting PRI_{norm}, normalized by both structural and chlorophyll indices exhibited the most robust results when tracking the diurnal trend of G_s.

The results obtained by the PRI_{norm} were comparable to thermal water-stress indices such as T_c-T_a and CWSI. As indicated in Table 3, the coefficients of determination for PRI_{norm} vs G_s were higher in all cases (when using only midday flights, and when all four flights were used together) when compared with T_c-T_a, which yielded coefficients of determination ranging between 0.74, $p < 0.01$ (13:00 h), and 0.59, $p < 0.001$ (all flights together). In the case of flights conducted during central hours, the CWSI yielded $r^2 = 0.74$, $p < 0.01$ at 13:00 h (Fig. 8a), and $r^2 = 0.77$, $p < 0.001$ for the two midday flights (Fig. 8b), while the PRI_{norm} obtained $r^2 = 0.81$, $p < 0.001$ and $r^2 = 0.79$, $p < 0.001$, respectively (Fig. 7). These results demonstrated that PRI_{norm} tracked the diurnal variation of G_s more accurately than the standard PRI formulation and, at the same time, showed a level of sensitivity similar to that of standard thermal indicators of water stress such as CWSI.

With regard to leaf water potential, the results obtained for all flights (Table 3) showed a similar and consistent behavior than G_s for all indices, with comparable levels of sensitivity. In summary, the conclusions would hold regarding the superior performance of the PRI_{norm} ($r^2 = 0.7$–0.8) vs PRI ($r^2 = 0.4$–0.5) for midday flights when compared to leaf water potential. Both T_c-T_a and the CWSI showed similar relationships against water potential than PRI_{norm} for the 13:00 + 15:30 h flight

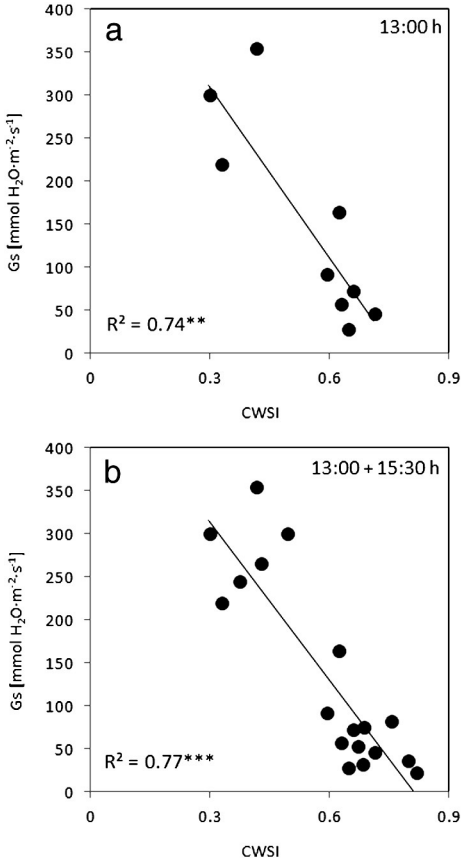

Fig. 8. Relationships obtained between stomatal conductance (G_s) and the Crop Water Stress Index (CWSI) for the flight conducted at 13:00 h (a) and for the two midday flights (b). Statistical significance is indicated as * ($p < 0.05$), ** ($p < 0.01$), and *** ($p < 0.001$).

($r^2 = 0.76$–0.78 for the three of them, $p < 0.001$), which diminished slightly when the 13:00 h flight was assessed on its own ($r^2 = 0.95$, $p < 0.001$ for CWSI and T_c-T_a; $r^2 = 0.82$, $p < 0.001$ for PRI_{norm}). Weaker relationships were obtained between water potential and structural indices NDVI and RDVI (both indices yielding $r^2 = 0.38$; $p < 0.01$ for 13:00 + 15:30 h), even for the single midday flight at 13:00 h ($r^2 = 0.34$; ns for NDVI) with higher performance for RDVI ($r^2 = 0.49$; $p < 0.05$). The red edge index R_{700}/R_{670} showed weaker sensitivity to water potential on single and multiple flights, with coefficients of determination in the range 0.14–0.17 (ns).

The sensitivity of the spectral indices benchmarked against CWSI, as indicators for water stress detection, demonstrated the robustness of the new PRI_{norm} index as compared to standard PRI and to structural formulations (Fig. 9). Moreover, PRI_{norm} yielded $r^2 = 0.77$, $p < 0.01$ against CWSI for the 13:00 h flight (Fig. 9a), while PRI ($r^2 = 0.42$; ns) (Fig. 9c) and NDVI ($r^2 = 0.3$; ns) (Fig. 9e), showed weaker relationships and were not statistically significant. Similar results were obtained for the two midday flights together (13:00 + 15:30 h) (Fig. 9b;d;f). As previously observed, the new PRI_{norm} index compared well against CWSI at the two central hours, when CWSI can be calculated and when sun angle effects were small on the multispectral indices. PRI_{norm} and PRI were highly significant ($p < 0.001$) when compared to CWSI, but PRI_{norm} obtained better results ($r^2 = 0.75$) than PRI ($r^2 = 0.58$). Therefore, the superior performance of PRI_{norm} was demonstrated not only against the diurnal dynamics of stomatal conductance and water potential at the leaf level, but also when assessed against the thermal-based CWSI index determined at the vine level.

In order to gain an understanding of the superior results obtained for PRI_{norm}, compared to the standard PRI index, the diurnal variation of G_s for each treatment (Fig. 10a) was compared with T_c-T_a (Fig. 10b), PRI

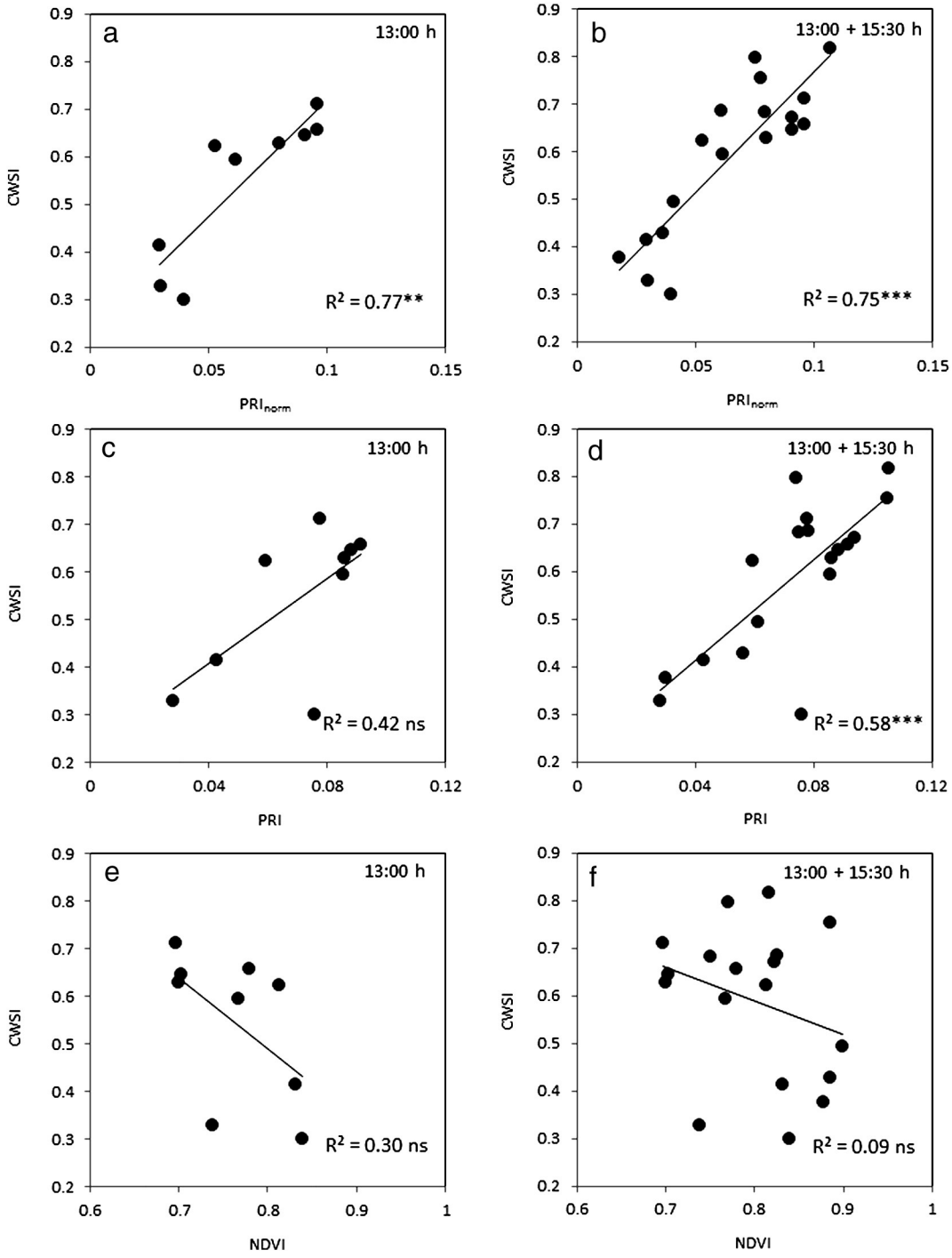

Fig. 9. Relationships obtained between Crop Water Stress Index (CWSI) and the index proposed in this study (PRI_{norm}) (a;b), the standard PRI (c;d), and the structural index NDVI (e;f) for the flight conducted at 13:00 h (a;c;e) and for the two midday flights together (b;d;f). Statistical significance is indicated as * ($p < 0.05$), ** ($p < 0.01$), and *** ($p < 0.001$).

(Fig. 10c), and PRI_{norm} (Fig. 10d). Results suggest that PRI was not able to differentiate between the intermediate and NI treatments (Fig. 10c), while both G_s and T_c-T_a reflected differences among treatments that were captured by PRI_{norm}. This result may partially explain the superior performance of the PRI index, when normalized by structure and chlorophyll effects, in distinguishing between irrigation treatments, which the standard PRI alone was unable to do.

4. Discussion

The treatments imposed in this study provided a wide range of vine water status for the development and validation of remote sensing indices to detect water stress in grapevines. The rate of water use in the IRR treatment, which was transpiring near maximum potential rate was almost four times more than that of the NI treatment. Both G_s and Ψ_{leaf} of the vines in the intermediate stressed (INT) and non-irrigated (NI) treatments indicated that they were more stressed compared to the IRR treatment (Table 2). Previous studies have demonstrated that the PRI index is sensitive to water stress levels, although it is affected by the confounding absorption of photosynthetic pigments, canopy structure, and background (Suarez et al., 2009, 2010). In controlled experiments where water stress levels are mild or imposed over short time periods, e.g. when imposing regulated deficit irrigation techniques, the effects of canopy structure and photosynthetic pigment

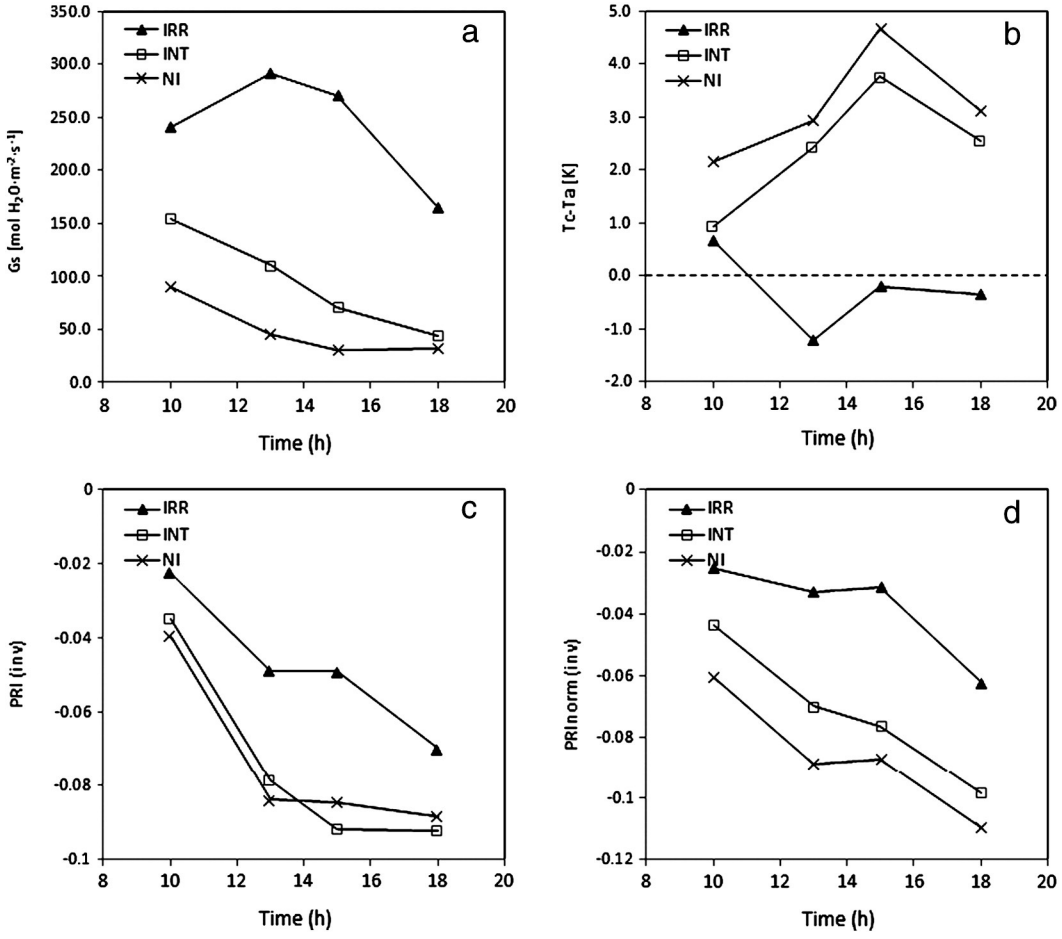

Fig. 10. Diurnal variation of G_s (a), T_c-T_a (b), PRI (c) and PRI_{norm} (d) over the course of the experiment. PRI and PRI_{norm} are shown inverted to improve clarity.

changes on the PRI index are low, and good sensitivity to stress is generally found (Suarez et al., 2010; Zarco-Tejada et al., 2012). In large, commercial, agricultural fields, the spatial variability of pigment concentration and canopy size and structure hinders operational use of the PRI index. These effects are problematic not only under real field conditions, but also in cases when different varieties are screened for genetic assessment and phenotyping, and plant breeding applications.

One of the major current limitations, in terms of modeling, is the lack of simulation of these effects using radiative transfer methods; currently, no simulation methods are available that allow for the diurnal dynamics of the xanthophyll cycle pigments and the confounding effects of chlorophyll, carotenoids, and anthocyanins, or the leaf area index, and structural, background and shading effects. The methods currently available to elucidate these effects on PRI rely on simulating the 531 nm and 570 nm spectral bands as a function of leaf pigment concentration and canopy structure variation; however, there is no proper assessment of the rapid conversion of pigments to a photoprotective form of the xanthophyll cycle pigments as a function of stress. Until a better modeling procedure is available, experimental studies need to be conducted to allow for this variability, and to determine its effects on the PRI index as a proxy for water stress.

In this paper, we show that PRI normalized by canopy chlorophyll content (RDVI and R_{700}/R_{670} being proxies for LAI and chlorophyll content, respectively) is better related to stomatal conductance and water potential than the standard PRI index in a diurnal experiment. The better performance of the normalized PRI index in tracking the diurnal dynamics of stomatal conductance could be due to different reasons. First, the PRI formulation proposed in this study is normalized by the total chlorophyll content of the canopy; accordingly, the PRI_{norm} may allow for limitations in transpiration, as a function of the photosynthetic capacity, under low chlorophyll content conditions (Farquhar & Wong, 1984). Second, the red edge index R_{700}/R_{670} used in this study to normalize PRI is calculated on the spectral bands affected by chlorophyll fluorescence emission (see Fig. 6 in Zarco-Tejada, Miller, Mohammed, & Noland, 2000; Fig. 4c in Zarco-Tejada, Miller, Mohammed, Noland, & Sampson, 2002). In fact, it might be that the index R_{700}/R_{670} used here is not only tracking changes in chlorophyll content, but is also sensitive to the diurnal variation of chlorophyll fluorescence emission, which is related to photosynthesis and to stomatal conductance (see Zarco-Tejada, Catalina, González, & Martín, 2013; Zarco-Tejada et al., 2012). Further experimental work is required to understand whether the effects of diurnal fluorescence on the R_{700}/R_{670} index are in fact playing a role in the normalized PRI index used here as an indicator of water stress.

In order to gain a better understanding of the results obtained from the index normalization proposed in this study, the effects of both higher LAI, and carotenoid and chlorophyll concentrations ($C_{xc} + C_{ab}$) on the linearity and saturation of PRI and PRI_{norm} were assessed. Simulations were made using PROSPECT + SAILH to model pure vegetation reflectance as a function of a gradient in leaf area index and pigment levels, observing the effects on both PRI and PRI_{norm} indices. The simulated scenarios were intended to mimic real conditions in the canopy under study, i.e. LAI ranging between 2 and 5, and simulating low (C_{ab} = 20 μg/cm^2; C_{xc} = 7 μg/cm^2), medium (C_{ab} = 50 μg/cm^2; C_{xc} = 11 μg/cm^2) and high (C_{ab} = 80 μg/cm^2; C_{xc} = 15 μg/cm^2) chlorophyll and carotenoid content levels. The simulations (normalized to the first case) showed that the PRI (Fig. 11a) saturates earlier than the PRI_{norm}

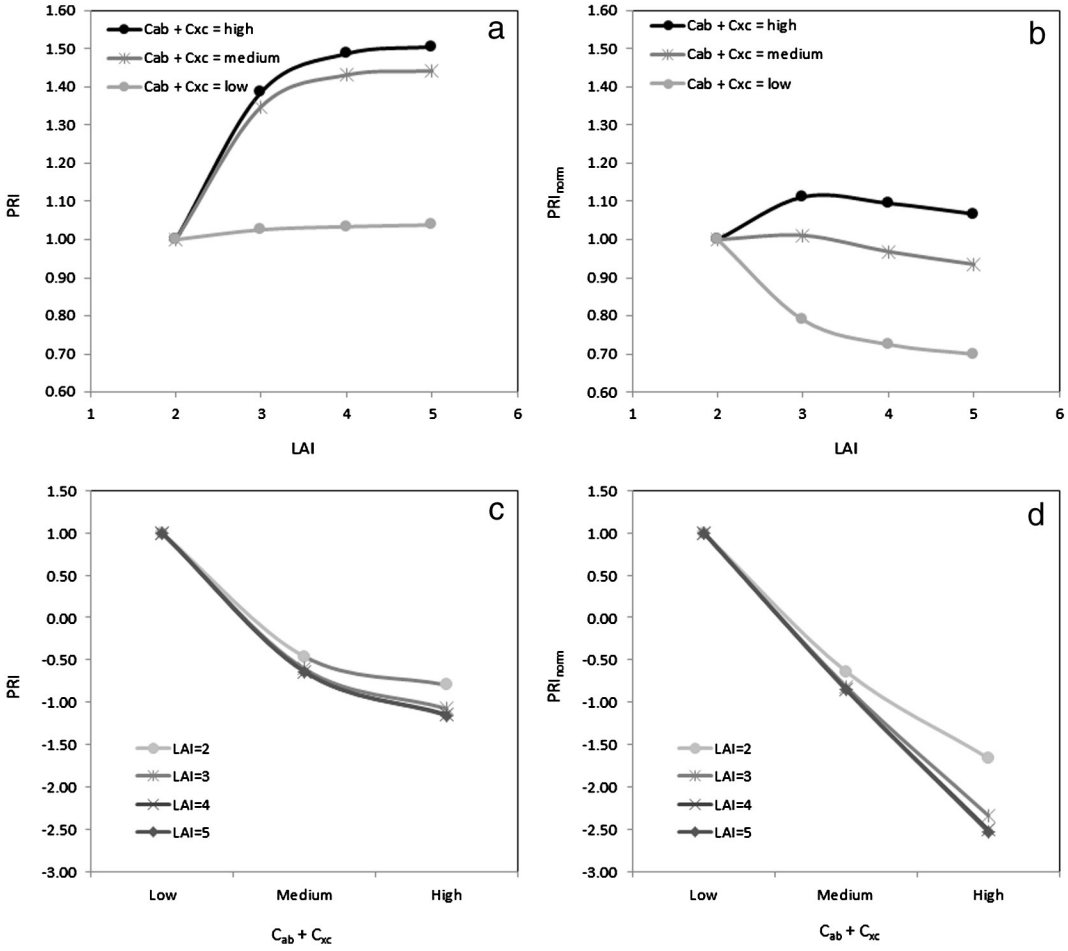

Fig. 11. Simulations conducted with PROSPECT + SAILH models to assess the effects of leaf area index (LAI) and pigment levels (carotenoids, C_{xc}; chlorophyll a + b, C_{ab}) on PRI (a;c) and on the normalized PRI index proposed in this study (PRI_{norm}) (b;d). The scenarios simulated comprised LAI ranging between 2 and 5, for low (C_{ab} = 20 μg/cm^2; C_{xc} = 7 μg/cm^2), medium (C_{ab} = 50 μg/cm^2; C_{xc} = 11 μg/cm^2) and high (C_{ab} = 80 μg/cm^2; C_{xc} = 15 μg/cm^2) chlorophyll and carotenoid content levels. Simulations were normalized to the first case scenario.

(Fig. 11b), as C_{xc} + C_{ab} content increases. The PRI trends for medium and high pigment levels were very close to each other, showing that the PRI decreases in sensitivity and reaches saturation at medium and high pigment levels. In contrast, the PRI_{norm} (Fig. 11b) was shown to be more sensitive to pigment content levels, probably because the PRI_{norm} is normalized by both structure and by the red edge chlorophyll-related index. Another important aspect observed is the linearity of PRI and PRI_{norm} with increasing pigment content levels. Specifically, saturation to medium and high pigment levels is clearly observed in PRI (Fig. 11c), while PRI_{norm} is more linear, especially for LAI values beyond 2 (Fig. 11d). In conclusion, the PRI_{norm} is more linearly related to increasing levels of pigment concentration, and at the same time, is weakly affected by LAI levels beyond 2. The viewing geometry (sun angle) effects were small in both PRI and PRI_{norm}, with changes in sun angle between 35° and 55° below 5% (data not shown).

In summary, this study shows that the PRI_{norm} is a more linearly-related index to canopy chlorophyll content levels than the standard PRI index, which may explain the better performance of the PRI_{norm} compared to the PRI when assessed against stomatal conductance and water potential. Therefore, the proposed PRI-based formulation, normalized by the red edge and structural indices, may effectively be more closely linked to the diurnal variation of stomatal conductance, as shown in the results on this experiment. The high similarity found between the PRI_{norm} and the thermal-based CWSI and T_c-T_a indices in the diurnal experiment shows that the PRI_{norm} modulates the physiological changes occurring in a canopy under different water stress levels better than the PRI. Further work would require the development of a physical model to simulate the diurnal dynamics of xanthophyll pigments, and the interaction between xanthophyll absorption and fluorescence emission on the PRI_{norm} index proposed in this study.

5. Conclusions

This study evaluated very high resolution narrow-band multispectral and thermal imagery acquired in a diurnal airborne experiment comprising three irrigation treatments for water stress detection. The assessment evaluated the diurnal relationships of a proposed PRI-based formulation (PRI_{norm}) that allows for variations of the structural and pigment content of the canopy, as compared to field-measured stomatal conductance and water potential. Concurrent acquisition of thermal imagery enabled computation of the widely accepted CWSI thermal index that is the established method for water stress detection, and was used here as a benchmark for both the proposed PRI-normalized index and the standard PRI formulation.

The results of the study demonstrate that, in the presence of structural and chlorophyll concentration effects that varied due to differences in vine water status, the standard PRI formulation was sensitive to water stress, but did not accurately track the diurnal dynamics of stomatal conductance and water potential. In the aforementioned conditions, the NDVI was a better indicator of water stress than the PRI, whenever relationships were obtained at a single timepoint, i.e. when all diurnal flights conducted throughout the experiment were not taken together. The study demonstrates that structure and pigment content (chlorophyll and carotenoids) need to be taken into account

when PRI is used as a proxy for diurnal variation of stomatal conductance and water potential. At midday, the combined PRI_{norm} index, based on the standard formulation of PRI normalized by RDVI (sensitive to structure) and R_{700}/R_{670} (sensitive to chlorophyll content, and potentially, to fluorescence emission) proved to be superior when compared against stomatal conductance ($r^2 = 0.79$; $p < 0.001$) and water potential ($r^2 = 0.77$; $p < 0.001$) than when using the standard PRI index (which obtained $r^2 = 0.52$ and 0.49, respectively). Furthermore, the PRI_{norm} and T_c-T_a tracked the diurnal dynamics of G_s better than PRI, when data from the four flights were taken together. The proposed PRI_{norm} index was highly related to the CWSI thermal index ($r^2 = 0.75$; $p < 0.001$), while the standard PRI obtained $r^2 = 0.58$ ($p < 0.001$). This strong relationship between PRI_{norm} and thermal-based indicators of water stress was also found on comparing T_c-T_a for the entire diurnal experiment, i.e. taking the data acquired at four timepoints during the day. Simulations showed that the PRI-normalized index proposed here saturates less to higher chlorophyll, carotenoid content and LAI levels, being more linearly related to canopy pigment content than the standard PRI formulation.

Acknowledgments

Authors acknowledge D. Notario, A. Vera, M. Salinas, and the staff of the University of California, Davis (UCD) for their technical support. This work was funded by the Spanish Ministry of Science and Innovation, under the projects CONSOLIDER CSD2006-0067 and AGL2009-13105.

References

Barton, C. V. M., & North, P. R. J. (2001). Remote sensing of canopy light use efficiency using the photochemical reflectance index. Model and analysis. *Remote Sensing of Environment*, *78*, 264–273.

Berni, J. A. J., Zarco-Tejada, P. J., Sepulcre-Cantó, G., Fereres, E., & Villalobos, F. (2009a). Mapping canopy conductance and CWSI in olive orchards using high resolution thermal remote sensing imagery. *Remote Sensing of Environment*, *113*, 2380–2388.

Berni, J. A. J., Zarco-Tejada, P. J., Suárez, L., & Fereres, E. (2009b). Thermal and narrowband multispectral remote sensing for vegetation monitoring from an unmanned aerial vehicle. *IEEE Transactions on Geoscience and Remote Sensing*, *47*(3), 722–738.

Damm, A., Erler, A., Hillen, W., Meroni, M., Schaepman, M. E., Verhoef, W., et al. (2011). Modeling the impact of spectral sensor configurations on the FLD retrieval accuracy of sun-induced chlorophyll fluorescence. *Remote Sensing of Environment*, *115*, 1882–1892.

Farquhar, G. D., & Wong, S.C. (1984). An empirical model of stomatal conductance. *Australian Journal of Plant Physiology*, *11*, 191–210.

Fereres, E., Cruz-Romero, G., Hoffman, G. F., & Rawlins, S. L. (1979). Recovery of orange trees following severe water stress. *Journal of Applied Ecology*, *16*, 833–842.

Fereres, E., & Soriano, M. (2007). Deficit irrigation for reducing agricultural water use. *Journal of Experimental Botany*, *58*, 147–159.

Flexas, J., Briantais, J. M., Cerovic, Z., Medrano, H., & Moya, I. (2000). Steady-state and maximum chlorophyll fluorescence responses to water stress in grapevine leaves: A new remote sensing system. *Remote Sensing of Environment*, *73*, 282–297.

Flexas, J., Escalona, J. M., Evain, S., Gulias, J., Moya, I., Osmond, C. B., et al. (2002). Steady-state chlorophyll fluorescence (Fs) measurements as a tool to follow variations of net CO_2 assimilation and stomatal conductance during water-stress in C-3 plants. *Physiologia Plantarum*, *114*(2), 231–240.

Flexas, J., Escalona, J. M., & Medrano, H. (1999). Water stress induces different levels of photosynthesis and electron transport rate regulation in grapevines. *Plant, Cell & Environment*, *22*, 39–48.

Gamon, J. A., Peñuelas, J., & Field, C. B. (1992). A narrow-wave band spectral index that tracks diurnal changes in photosynthetic efficiency. *Remote Sensing of Environment*, *41*, 35–44.

Gonzalez-Dugo, V., Zarco-Tejada, P. J., Berni, J. A., Suarez, L., Goldhamer, D., & Fereres, E. (2012). Almond tree canopy temperature reveals intra-crown variability that is water stress-dependent. *Agricultural and Forest Meteorology*, *154–155*, 156–165.

Grimes, D. W., & Williams, L. E. (1990). Irrigation effects on plant water relations and productivity of Thompson seedless grapevines. *Crop Science*, *30*, 255–260.

Gueymard, C. A. (2005). SMARTS code, version 2.9.5 user's manual solar consulting services. Online PDF document from. http://www.nrel.gov/rredc/smarts/

Guillén-Climent, M. L., Zarco-Tejada, P. J., Berni, J. A. J., North, P. R. J., & Villalobos, F. J. (2012). Mapping radiation interception in row-structured orchards using 3D simulation and high resolution airborne imagery acquired from a UAV. *Precision Agriculture*, *13*, 473–500.

Haboudane, D., Miller, J. R., Tremblay, N., Zarco-Tejada, P. J., & Dextraze, L. (2002). Integrated narrow-band vegetation indices for prediction of crop chlorophyll content for application to precision agriculture. *Remote Sensing of Environment*, *84*, 416–426.

Hall, A. E., Camacho-B, S. E., & Kaufmann, M. R. (1975). Regulation of water loss by citrus leaves. *Physiologia Plantarum*, *33*, 62–65.

Hall, F. G., Hilker, T., Coops, N. C., Lyapustin, A., Huemmrich, K. F., Middleton, E. M., et al. (2008). Multi-angle remote sensing of forest light use efficiency by observing PRI variation with canopy shadow fraction. *Remote Sensing of Environment*, *112*, 3201–3211.

Hernández-Clemente, R., Navarro-Cerrillo, R., Suárez, L., Morales, F., & Zarco-Tejada, P. J. (2011). Assessing structural effects on PRI for stress detection in conifer forests. *Remote Sensing of Environment*, *115*(9), 2360–2375.

Hilker, T., Coops, N. C., Hall, F. G., Black, T. A., Wulder, M.A., Nesic, Z., et al. (2008). Separating physiologically and directionally induced changes in PRI using BRDF models. *Remote Sensing of Environment*, *112*, 2777–2788.

Idso, S. B., Jackson, R. D., Pinter, P. J. J., Reginato, R. J., & Hatfield, J. L. (1981). Normalizing the stress degree-day parameter for environmental variability. *Agricultural Meteorology*, *24*, 45–55.

Idso, S. B., Jackson, R. D., & Reginato, R. J. (1978). Extending the "degree day" concept of plant phenological development to include water stress effects. *Ecology*, *59*, 431–433.

Jackson, R., Idso, S., Reginato, R., & Pinter, P. J. (1981). Canopy temperature as a crop water stress indicator. *Water Resources Research*, *17*, 1133–1138.

Jones, H. G. (1992). *Plants and microclimate: A quantitative approach to environmental plant physiology*. Cambridge: Cambridge University Press.

Krause, G. H., & Weis, E. (1984). Chlorophyll fluorescence as a tool in plant physiology. II. Interpretation of fluorescence signals. *Photosynthesis Research*, *5*, 139–157.

Larcher, W. (1994). Photosynthesis as a tool for indicating temperature stress events. In E. D. Schulze, & M. M. Caldwell (Eds.), *Ecophysiology of photosynthesis* (pp. 261–277). Berlin: Springer.

Leinonen, I., & Jones, H. G. (2004). Combining thermal and visible imagery for estimating canopy temperature and identifying plant stress. *Journal of Experimental Botany*, *55*(401), 1423–1431.

Lichtenthaler, H. K. (1992). The Kautsky effect: 60 years of chlorophyll fluorescence induction kinetics. *Photosynthetica*, *27*, 45–55.

Lichtenthaler, H. K., & Rinderle, U. (1988). The role of chlorophyll fluorescence in the detection of stress conditions in plants. *CRC Critical Reviews in Analytical Chemistry*, *19*(Suppl. 1), 529–585.

Meggio, F., Zarco-Tejada, P. J., Núñez, L. C., Sepulcre-Cantó, G., Gonzalez, M. R., & Martin, P. (2010). Grape quality assessment in vineyards affected by iron deficiency chlorosis using narrow-band physiological remote sensing indices. *Remote Sensing of Environment*, *114*, 1968–1986.

Meroni, M., Colombo, R., & Cogliati, S. (2004). High resolution leaf spectral signature for the detection of solar induced chlorophyll fluorescence. *Proceedings of the 2nd ESA workshop on remote sensing of solar induced vegetation fluorescence, Montreal, Canada, 17–19 November 2004*.

Meroni, M., Picchi, V., Rossini, M., Cogliati, S., Panigada, C., Nali, C., et al. (2008a). Leaf level early assessment of ozone injuries by passive fluorescence and PRI. *International Journal of Remote Sensing*, *29*(17), 5409–5422.

Meroni, M., Rossini, M., Guanter, L., Alonso, L., Rascher, U., & Colombo, R. (2009). Remote sensing of solar-induced chlorophyll fluorescence: Review of methods and applications. *Remote Sensing of Environment*, *113*, 2037–2051.

Meroni, M., Rossini, M., Picchi, V., Panigada, C., Cogliati, S., Nali, C., et al. (2008b). Assessing steady-state fluorescence and PRI from hyperspectral proximal sensing as early indicators of plant stress: The case of ozone exposure. *Sensors*, *8*, 1740–1754.

Middleton, E. M., Cheng, Y. B., Hilker, T., Black, T. A., Krishnan, P., Coops, N. C., et al. (2009). Linking foliage spectral responses to canopy level ecosystem photosynthetic light use efficiency at a Douglas-fir forest in Canada. *Canadian Journal of Remote Sensing*, *35*, 166–188.

Miyashita, K., Tanakamaru, S., Maitani, T., & Kimura, K. (2005). Recovery responses of photosynthesis, transpiration, and stomatal conductance in kidney bean following drought stress. *Environmental and Experimental Botany*, *53*, 205–214.

Moran, M. S., Clarke, T. R., Inoue, Y., & Vidal, A. (1994). Estimating crop water deficit using the relation between surface-air temperature and spectral vegetation index. *Remote Sensing of Environment*, *49*, 246–263.

Moya, I., Camenen, L., Evain, S., Goulas, Y., Cerovic, Z. G., & Latouche, G. (2004). A new instrument for passive remote sensing 1. Measurements of sunlight-induced chlorophyll fluorescence. *Remote Sensing of Environment*, *91*, 186–197.

Papageorgiou, G. (1975). Chlorophyll fluorescence: An intrinsic probe of photosynthesis. In Govindjee (Ed.), *Bioenergetics of photosynthesis* (pp. 319–371). New York: Academic Press.

Peguero-Pina, J. J., Morales, F., Flexas, J., Gil-Pelegrín, E., & Moya, I. (2008). Photochemistry, remotely sensed physiological reflectance index and de-epoxidation state of the xanthophyll cycle in *Quercus coccifera* under intense drought. *Oecologia*, *156*(1), 1–11.

Rondeaux, G., Steven, M., & Baret, F. (1996). Optimization of soil-adjusted vegetation indices. *Remote Sensing of Environment*, *55*, 95–107.

Rougean, J. -L., & Breon, F. M. (1995). Estimating PAR absorbed by vegetation from bidirectional reflectance measurements. *Remote Sensing of Environment*, *51*, 375–384.

Rouse, J. W., Haas, R. H., Schell, J. A., Deering, D. W., & Harlan, J. C. (1974). Monitoring the vernal advancements and retrogradation of natural vegetation. In U. G. MD (Ed.), *Nasa/Gsfc final report* (pp. 371).

Schreiber, U., & Bilger, W. (1987). Rapid assessment of stress effects on plant leaves by chlorophyll fluorescence measurements. In J.D. Tenhunen, & E. M. Catarino (Eds.), *Plant response to stress* (pp. 27–53). Berlin, Germany: Springer-Verlag.

Schreiber, U., Bilger, W., & Neubauer, C. (1994). Chlorophyll fluorescence as a non-intrusive indicator for rapid assessment of in vivo photosynthesis. In E. D. Schulze, & M. M. Caldwell (Eds.), *Ecophysiology of photosynthesis. Ecological studies, vol. 100*. (pp. 49–70). Berlin Heidelberg New York: Springer.

Sepulcre-Cantó, G., Zarco-Tejada, P. J., Jiménez-Muñoz, J. C., Sobrino, J. A., Miguel, E. D., & Villalobos, F. J. (2006). Detection of water stress in an olive orchard with thermal remote sensing imagery. *Agricultural and Forest Meteorology*, *136*(1–2), 31–44.

Sepulcre-Cantó, G., Zarco-Tejada, P. J., Jiménez-Muñoz, J. C., Sobrino, J. A., Soriano, M.A., Fereres, E., et al. (2007). Monitoring yield and fruit quality parameters in open-canopy

tree crops under water stress. Implications for ASTER. *Remote Sensing of Environment*, *107*, 455–470.

Stagakis, S., González-Dugo, V., Cid, P., Guillén-Climent, M. L., & Zarco-Tejada, P. J. (2012). Monitoring water stress and fruit quality in an orange orchard under regulated deficit irrigation using narrow-band structural and physiological remote sensing indices. *ISPRS Journal of Photogrammetry and Remote Sensing*, *71*, 47–61.

Suarez, L., Zarco-Tejada, P. J., Berni, J. A. J., González-Dugo, V., & Fereres, E. (2009). Modelling PRI for water stress detection using radiative transfer models. *Remote Sensing of Environment*, *113*, 730–744.

Suarez, L., Zarco-Tejada, P. J., González-Dugo, V., Berni, J. A. J., Sagardoy, R., Morales, F., et al. (2010). Detecting water stress effects on fruit quality in orchards with time-series PRI airborne imagery. *Remote Sensing of Environment*, *114*, 286–298.

Suarez, L., Zarco-Tejada, P. J., Sepulcre-Cantó, G., Pérez-Priego, O., Miller, J. R., Jiménez-Muñoz, J. C., et al. (2008). Assessing canopy PRI for water stress detection with diurnal airborne imagery. *Remote Sensing of Environment*, *112*, 560–575.

Thenot, F., Méthy, M., & Winkel, T. (2002). The Photochemical Reflectance Index (PRI) as a water-stress index. *International Journal of Remote Sensing*, *23*(23), 5135–5139.

Villalobos, F. J., Testi, L., & Moreno-Perez, M. F. (2008). Evaporation and canopy conductance of citrus orchard. *Agricultural Water Management*, *96*(4), 565–573.

Williams, L. E., & Araujo, F. (2002). Correlations among predawn leaf, midday leaf, and midday stem water potential and their correlations with other measures of soil and plant water status in *Vitis vinifera* L. *Journal of the American Society for Horticultural Science*, *127*, 448–454.

Williams, L. E., Baeza, P., & Vaughn, P. (2012). Midday measurements of leaf water potential and stomatal conductance are highly correlated with daily water use of Thompson Seedless grapevines. *Irrigation Science*, *30*(3), 201–212.

Williams, L. E., Grimes, D. W., & Phene, C. J. (2010). The effects of applied water at various fractions of measured evapotranspiration on water relations and vegetative growth of Thompson Seedless. *Irrigation Science*, *28*, 221–232.

Williams, L. E., Phene, C. J., Grimes, D. W., & Trout, T. J. (2003). Water use of mature Thompson Seedless grapevines in California. *Irrigation Science*, *22*(1), 11–18.

Williams, L. E., & Trout, T. J. (2005). Relationships among vine and soil based measures of water status in a Thompson Seedless vineyard in response to high frequency drip irrigation. *American Journal of Enology and Viticulture*, *56*, 357–366.

Zarco-Tejada, P. J., Catalina, A., González, M. R., & Martín, P. (2013). Relationships between net photosynthesis and steady-state chlorophyll fluorescence retrieved from airborne hyperspectral imagery. *Remote Sensing of Environment*, *136*, 247–258.

Zarco-Tejada, P. J., González-Dugo, V., & Berni, J. A. J. (2012). Fluorescence, temperature and narrow-band indices acquired from a UAV platform for water stress detection using a micro-hyperspectral imager and a thermal camera. *Remote Sensing of Environment*, *117*, 322–337.

Zarco-Tejada, P. J., Guillén-Climent, M. L., Hernández-Clemente, R., Catalina, A., González, M. R., & Martín, P. (2013b). Estimating leaf carotenoid content in vineyards using high resolution hyperspectral imagery acquired from an unmanned aerial vehicle. *Agricultural and Forest Meteorology*, *171–172*, 281–294.

Zarco-Tejada, P. J., Miller, J. R., Mohammed, G. H., & Noland, T. L. (2000). Chlorophyll fluorescence effects on vegetation apparent reflectance: I. Leaf-level measurements and model simulation. *Remote Sensing of Environment*, *74*(3), 582–595.

Zarco-Tejada, P. J., Miller, J. R., Mohammed, G. H., Noland, T. L., & Sampson, P. H. (2002). Vegetation stress detection through chlorophyll a + b estimation and fluorescence effects on hyperspectral imagery. *Journal of Environmental Quality*, *31*, 1433–1441.